Non-linear Finite Element Analysis of CRTS Reflectors

C.Y. Lai and S. Pellegrino

CUED/D-STRUCT/TR192

European Space Agency Contractor Report

The work presented in this report was carried out under an ESA contract.

Responsibility for its contents resides with the authors.

ESA Study Manager: W.J. Rits

ESTEC Contract no. 11936/96/NL/FG

Release date: 16 March 2001

Abstract

This report presents a non-linear finite element simulation of the assembly process of a collapsible rib-tensioned surface (CRTS) reflector, leading to estimates of its surface accuracy and prestress distribution. In two previous reports in this series preliminary estimates had been obtained by a linearised formulation; hence the main aim of the present study is to access the accuracy of estimates based on the earlier method.

Carrying out a fully non-linear simulation of an offset CRTS reflector is a formidable computational challenge, which has required the development of special purpose software. Despite this, only for a limited set of test cases it has been possible to achieve full convergence.

A complete non-linear simulation of an 8-rib offset reflector with focal length of 0.9 m and diameter of 1 m is presented and the results are compared to the linear analysis. It turns out that the RMS surface errors predicted by the two methods are practically identical but the stress magnitudes are less accurate, due to incomplete modelling of the sliding between the membrane and the cables and ribs of the reflector.

It is concluded that the linearised method presented in the earlier reports is a very good way of determining the actual prestressed shape of a CRTS reflector.

Contents

List of Tables

List of Figures

Chapter 1

Introduction

The previous two reports in this series (Lai, You and Pellegrino 1997, Lai and Pellegrino 1999) have presented a methodology for the design of collapsible rib-tensioned surface (CRTS) reflectors. A key stage in the design process is the computation of the cutting pattern for the gores of the reflector, after which an elastic analysis is carried out to determine the actual prestressed shape of a reflector made from these gores.

Lai, You and Pellegrino (1997) have proposed a linear-elastic analysis to find this actual shape, taking the equilibrium surface as a reference and setting up a linearised stiffness matrix in this configuration. Thus, the initial shape is obtained as a small variation from this configuration. However, this linear approach requires the shape distortion to be small and, since this cannot be guaranteed in all cases, a full non-linear finite element analysis scheme has been set up, to verify the results from the simpler method.

The non-linear finite-element formulation by Tabarrok and Qin (1992) has been adopted and the present implementation has been validated against the classical solution (Hencky 1915) for the deflection of a circular membrane — initially without any tension— subjected to a uniform pressure.

To obtain an accurate estimate of the shape and stress distribution in a particular CRTS reflector, the simulation approach presented in this report simulates the final stages of its assembly process, as follows. First, the gores of the reflector, whose edges are cut according to a cutting pattern determined according to the earlier reports, are laid out flat in a common plane, unjointed. Then, they are rotated, each as a rigid body, into their approximate final positions. Next, the gores are joined to the ribs, which are initially assumed to be rigid and then allowed to deform elastically under the forces applied by the membrane, while a series of equilibrium iterations are carried out.

1.1 Layout of the Report

This report is divided into five chapters.

Following this brief introduction, Chapters 2 and 3 form the main body of the report: the non-linear finite element formulation of the three elements that form the reflector, namely membrane, cables, and ribs, is presented in Chapter 2. The procedure that simulates the assembly process of the whole structure is presented in Chapter 3.

Chapter 4 presents the results of this simulation for reflectors with 8 and 12 ribs. Intermediate results at each stage of the analysis are presented, but the analysis of the 12 rib reflector has convergence problem in the final stages, and so final results are obtained only for the 8 rib reflector. These results are compared with the results from the linear analysis of the same reflector, from Lai, You and Pellegrino (1997).

Chapter 2

Formulation

The determination of the shape of a prestressed CRTS reflector surface involves satisfying the equilibrium equations of three different structural elements: membrane, cable and beam elements. Membrane and cable elements are assumed to have zero flexural stiffness and hence will readily change their curvature in response to most applied loads; therefore, large deflection theory is required for their analysis. On the other hand, the curved ribs can be modelled as a series of straight beam elements of uniform cross-section; because the ribs behave linearly within the deflection range of interest, small deflection theory is adequate.

The non-linear finite element formulation that has been adopted for the membrane and cable elements is that proposed by Tabarrok and Qin (1992), and the overall solution procedure is a standard Newton-Raphson. Readers interested in further details on the analysis are referred to the paper by Tabarrok and Qin, and textbooks such as Crisfield (1991) and Belytschko *et al.* (2000).

2.1 Membrane Element

In geometrically non-linear finite element analysis it is generally preferable to use a larger number of lower order elements than a smaller number of higher order elements. Hence, the element that will be used is a three-node, linear displacement field, constant stress triangular element with nine degrees of freedom. The formulation that is presented in this section is suitable for an iterative solution of the stiffness equations of the membrane, taking into account the non-linearity of the interaction between the shape change of the membrane and the loads applied to it.

Figure 2.1 shows a triangular membrane element in three-dimensional space. The X, Y, Z axes represent the global coordinate system; a local coordinate system x, y, z is used to formulate the element matrices.

The linear displacement field, $u(x, y)$, $v(x, y)$, and $w(x, y)$, of the element can

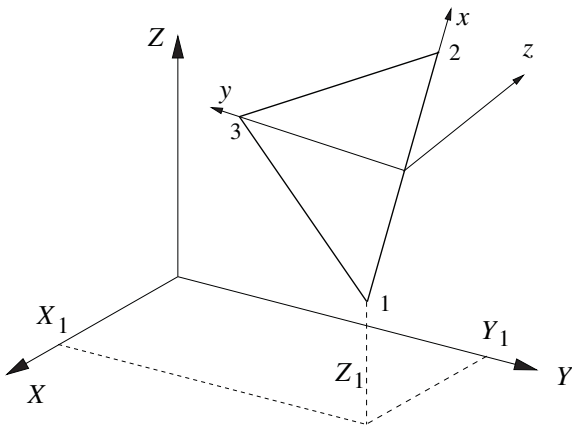

Figure 2.1: Coordinate system of 3 node membrane element.

be expressed as

$$\begin{aligned} u &= \alpha_1 + \alpha_2 x + \alpha_3 y \\ v &= \alpha_4 + \alpha_5 x + \alpha_6 y \\ w &= \alpha_7 + \alpha_8 x + \alpha_9 y \end{aligned} \tag{2.1}$$

where the nine α_i coefficients are not specified. It is preferable to convert the α_i's to the nine nodal displacements

$$\mathbf{u} = [u_1 \;\; v_1 \;\; w_1 \;\; u_2 \;\; v_2 \;\; w_2 \;\; u_3 \;\; v_3 \;\; w_3]^T$$

Determining the displacements at the three nodes and solving for α_i leads to the three shape functions of the element, using which Equation 2.1 becomes

$$\begin{aligned} u &= (a_1 + b_1 x + c_1 y)u_1 + (a_2 + b_2 x + c_2 y)u_2 + (a_3 + b_3 x + c_3 y)u_3 \\ v &= (a_1 + b_1 x + c_1 y)v_1 + (a_2 + b_2 x + c_2 y)v_2 + (a_3 + b_3 x + c_3 y)v_3 \\ w &= (a_1 + b_1 x + c_1 y)w_1 + (a_2 + b_2 x + c_2 y)w_2 + (a_3 + b_3 x + c_3 y)w_3 \end{aligned} \tag{2.2}$$

where

$$\begin{aligned} a_1 &= (x_2 y_3 - x_3 y_2)/2\triangle, \quad b_1 = (y_2 - y_3)/2\triangle, \quad c_1 = (x_3 - x_2)/2\triangle \\ a_2 &= (x_3 y_1 - x_1 y_3)/2\triangle, \quad b_2 = (y_3 - y_1)/2\triangle, \quad c_2 = (x_1 - x_3)/2\triangle \\ a_3 &= (x_1 y_2 - x_2 y_1)/2\triangle, \quad b_3 = (y_1 - y_2)/2\triangle, \quad c_3 = (x_2 - x_1)/2\triangle \end{aligned}$$

and $\triangle$ = element area.

A membrane element is not able to sustain any flexural stresses, which means that only the stresses tangent to the curved membrane surface act to equilibrate loads normal to it. As the loads change, the stresses and the local curvatures change to maintain equilibrium and these changes are accompanied by significant displacements and rotations of the surface. Therefore, small-deflection theory is

not applicable, but the quadratic terms in the displacement-strain relations must be taken into account. The nonlinear displacement-strain relations are (Love 1944)

$$\begin{aligned}
\epsilon_x &= \frac{\partial u}{\partial x} + \frac{1}{2}\left[\left(\frac{\partial u}{\partial x}\right)^2 + \left(\frac{\partial v}{\partial x}\right)^2 + \left(\frac{\partial w}{\partial x}\right)^2\right] \\
\epsilon_y &= \frac{\partial u}{\partial y} + \frac{1}{2}\left[\left(\frac{\partial u}{\partial y}\right)^2 + \left(\frac{\partial v}{\partial y}\right)^2 + \left(\frac{\partial w}{\partial y}\right)^2\right] \\
\gamma_{xy} &= \frac{\partial u}{\partial y} + \frac{\partial v}{\partial x} + \left[\frac{\partial u}{\partial x}\frac{\partial u}{\partial y} + \frac{\partial v}{\partial x}\frac{\partial v}{\partial y} + \frac{\partial w}{\partial x}\frac{\partial w}{\partial y}\right]
\end{aligned} \tag{2.3}$$

Substituting Equation 2.2 into 2.3 and writing the outcome in matrix form gives

$$\boldsymbol{\epsilon} = \mathbf{B_0}\mathbf{u} + \frac{1}{2}\mathbf{A}\boldsymbol{\theta} \tag{2.4}$$

where

$$\begin{aligned}
\mathbf{B_0} &= \begin{bmatrix} b_1 & 0 & 0 & b_2 & 0 & 0 & b_3 & 0 & 0 \\ 0 & c_1 & 0 & 0 & c_2 & 0 & 0 & c_3 & 0 \\ c_1 & b_1 & 0 & c_2 & b_2 & 0 & c_3 & b_3 & 0 \end{bmatrix} \\
\mathbf{A} &= \begin{bmatrix} \partial u/\partial x & \partial v/\partial x & \partial w/\partial x & 0 & 0 & 0 \\ 0 & 0 & 0 & \partial u/\partial y & \partial v/\partial y & \partial w/\partial y \\ \partial u/\partial y & \partial v/\partial y & \partial w/\partial y & \partial u/\partial x & \partial v/\partial x & \partial w/\partial x \end{bmatrix} \\
\boldsymbol{\theta} &= \begin{bmatrix} \partial u/\partial x & \partial v/\partial x & \partial w/\partial x & \partial u/\partial y & \partial v/\partial y & \partial w/\partial y \end{bmatrix}^T
\end{aligned}$$

The change of strain $\delta\boldsymbol{\epsilon}$ due to infinitesimal nodal displacements $\delta\mathbf{u}$ is obtained by differentiation of Equation 2.4. Considering the above expressions for $\mathbf{A}$ and $\boldsymbol{\theta}$, this gives

$$\delta\boldsymbol{\epsilon} = (\mathbf{B_0} + \mathbf{AG})\delta\mathbf{u} \tag{2.5}$$

where

$$\mathbf{G} = \begin{bmatrix} b_1 & 0 & 0 & b_2 & 0 & 0 & b_3 & 0 & 0 \\ 0 & b_1 & 0 & 0 & b_2 & 0 & 0 & b_3 & 0 \\ 0 & 0 & b_1 & 0 & 0 & b_2 & 0 & 0 & b_3 \\ c_1 & 0 & 0 & c_2 & 0 & 0 & c_3 & 0 & 0 \\ 0 & c_1 & 0 & 0 & c_2 & 0 & 0 & c_3 & 0 \\ 0 & 0 & c_1 & 0 & 0 & c_2 & 0 & 0 & c_3 \end{bmatrix}$$

By differentiating Equation 2.2, it can be shown that $\boldsymbol{\theta}$ has the following expression in terms of the nodal variables

$$\boldsymbol{\theta} = \mathbf{G}\mathbf{u}$$

Since only small strains are of interest, despite the displacements being relatively large, the constitutive relations for linear-elastic plane stress analysis may be used. Thus

$$\boldsymbol{\sigma} = \mathbf{D}\boldsymbol{\epsilon} + \boldsymbol{\sigma_0} \tag{2.6}$$

where $\boldsymbol{\sigma_0}$ denotes the initial stress vector and $\mathbf{D}$ is the elastic matrix defined as

$$\mathbf{D} = \frac{E}{1-\nu^2}\begin{bmatrix} 1 & \nu & 0 \\ \nu & 1 & 0 \\ 0 & 0 & \frac{1-\nu}{2} \end{bmatrix}$$

where E and ν are the Young's Modulus and Poisson's ratio, respectively.

Using the principle of virtual work, the following equilibrium equations are established for a single element in its local coordinate system

$$\int_{V^e} \delta\boldsymbol{\epsilon}^T \boldsymbol{\sigma} dV - \delta\mathbf{u}^T\mathbf{p} = 0 \tag{2.7}$$

where V^e denotes the element volume and $\mathbf{p}$ is the external nodal force vector, in the local coordinate system.

Substituting Equations 2.4 - 2.6 into 2.7 and eliminating $\delta\mathbf{u}^T$ gives the following local equilibrium equations for a membrane element

$$\int_{V^e} (\mathbf{B_0} + \mathbf{AG})^T[\mathbf{D}(\mathbf{B_0u} + \frac{1}{2}\mathbf{A}\boldsymbol{\theta}) + \boldsymbol{\theta_0}]dV - \mathbf{p} = 0 \tag{2.8}$$

These equations must be transformed into the global coordinate system and, proceeding in the same way for all membrane elements in the surface, a set of global equilibrium equations can be obtained.

Since these equations will be used within an iterative solution based on the Newton-Raphson method, they have to be linearised at the element level. Let the out-of-balance forces be $\boldsymbol{\phi}^i$ at the end of iteration i

$$\boldsymbol{\phi}^i = \int_{V^e} (\mathbf{B_0} + \mathbf{A}^i\mathbf{G})^T[\mathbf{D}(\mathbf{B_0u}^i + \frac{1}{2}\mathbf{A}^i\boldsymbol{\theta}^i) + \boldsymbol{\theta_0}]dV - \mathbf{p} \tag{2.9}$$

The nodal displacements $\delta\mathbf{u}^i$ that are required to correct for these out-of-balance forces are such that

$$\boldsymbol{\phi}^{i+1} = \boldsymbol{\phi}^i + \frac{\partial\boldsymbol{\phi}^i}{\partial\mathbf{u}}\delta\mathbf{u}^i = 0 \tag{2.10}$$

Thus, the displacements after iteration $i+1$ can be obtained by solving Equation 2.10 and then updating the displacements

$$\mathbf{u}^{i+1} = \mathbf{u}^i + \delta\mathbf{u}^i \tag{2.11}$$

Noting that Equation 2.10 provides a relationship between the change in nodal forces, $\boldsymbol{\phi}^{i+1} - \boldsymbol{\phi}^i$, and the corresponding nodal displacements, $\mathbf{u}^i$, it follows that

the matrix relating the two, $\partial\boldsymbol{\phi}^i/\partial\mathbf{u}$, is the *tangent stiffness matrix* for then element. It consists of two parts, as follows

$$\begin{aligned}
\mathbf{k}^i &= \frac{\partial\boldsymbol{\phi}^i}{\partial\mathbf{u}} \\
&= \int_{V^e}(\mathbf{B_0}+\mathbf{A}^i\mathbf{G})^T\frac{\partial}{\partial\mathbf{u}}[\mathbf{D}(\mathbf{B_0}\mathbf{u}^i+\frac{1}{2}\mathbf{A}^i\boldsymbol{\theta}^i)]dV \\
&\quad+\int_{V^e}\frac{\partial}{\partial\mathbf{u}}[(\mathbf{B_0}+\mathbf{A}^i\mathbf{G})^T]\times[\mathbf{D}(\mathbf{B_0}\mathbf{u}^i+\frac{1}{2}\mathbf{A}^i\boldsymbol{\theta}^i)+\boldsymbol{\theta}_0]dV \\
&= \int_{V^e}(\mathbf{B_0}+\mathbf{A}^i\mathbf{G})^T\mathbf{D}(\mathbf{B_0}+\mathbf{A}^i\mathbf{G})dV+\int_{V^e}\mathbf{G}^T\mathbf{M}^i\mathbf{G}dV \qquad (2.12)\\
&= \mathbf{k}_e^i+\mathbf{k}_g^i
\end{aligned}$$

where $\mathbf{k}_e^i$ and $\mathbf{k}_g^i$ are the material and geometric stiffness matrices in local coordinates, respectively, and

$$\mathbf{M}^i=\begin{bmatrix}\sigma_{xx}&0&0&\tau_{xy}&0&0\\0&\sigma_{xx}&0&0&\tau_{xy}&0\\0&0&\sigma_{xx}&0&0&\tau_{xy}\\\tau_{xy}&0&0&\sigma_{yy}&0&0\\0&\tau_{xy}&0&0&\sigma_{yy}&0\\0&0&\tau_{xy}&0&0&\sigma_{yy}\end{bmatrix}$$

Note that the geometric stiffness of an initially unstressed membrane is zero as $\mathbf{M}^i=0$. If the membrane is also initially flat, and hence its out-of-plane material stiffness is also zero, there will be a singularity at the beginning of the equilibrium iteration. This can be avoided by prescribing an initial, small out-of-plane displacement of the membrane before starting the standard Newton-Raphson iteration.

2.2 Validation against Hencky's Solution

The computer implementation of the membrane element described in the previous section has been validated against the classical analytical solution for the deflection of a linear-elastic, circular membrane supported by a rigid foundation. The membrane is initially unstressed. This problem was first solved by Hencky (1915); later, Campbell (1956) corrected a numerical error made by Hencky.

Hencky showed that the vertical deflection of an initially horizontal membrane of outer radius a and subject to pressure p is given by

$$w=a\left(\frac{pa}{Et}\right)^{\frac{1}{3}}f(r) \qquad (2.13)$$

where E is the Young's Modulus of the membrane, t its thickness, r the distance from the centre, and $f(r)$ a function of r which has the expression

$$f(r)=A_0+A_2\left(\frac{r}{a}\right)^2+A_4\left(\frac{r}{a}\right)^4+A_6\left(\frac{r}{a}\right)^6\ldots \qquad (2.14)$$

where

$$\begin{aligned} B_0 &= 1.724^* & A_0 &= 0.653, \\ A_2 &= -1/B_0, & A_4 &= -1/2B_0^4, \\ A_6 &= -5/9B_0^7, & A_8 &= -55/72B_0^{10}, \\ A_{10} &= -7/6B_0^{13}, & A_{12} &= -205/108B_0^{16}, \text{ etc.} \end{aligned}$$

Figure 2.2 shows the deflected shape of such a membrane, divided up into 16 elements. The membrane is fixed along its edge, therefore nodes 11 - 15 are fully constrained. Only a quarter of the complete membrane has been analysed, and therefore symmetry boundary conditions are applied to node 1 (constrained in the X- and Y-direction), nodes 2,4, 7 (constrained in the Y-direction only), and nodes 3, 6,10 (constrained in the X–direction only).

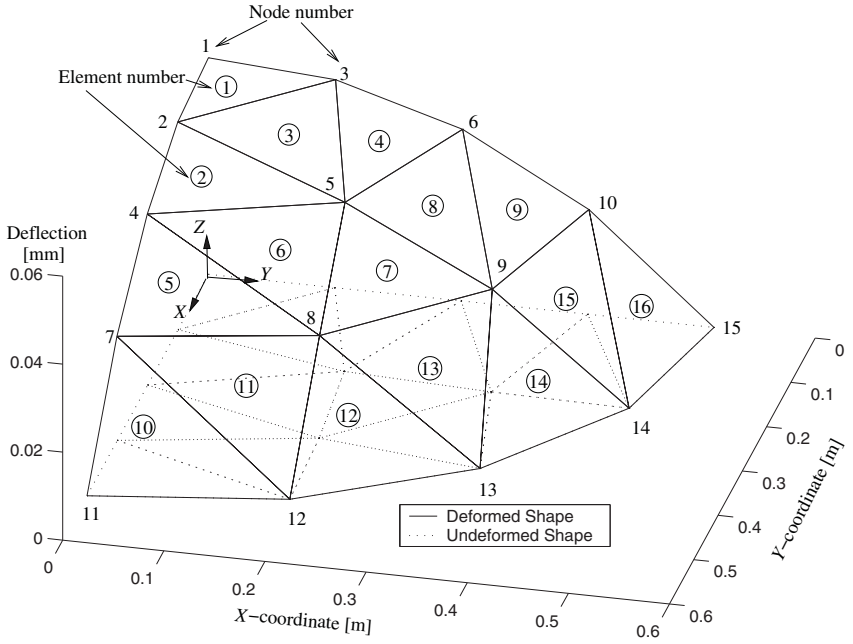

Figure 2.2: Deflection of circular membrane under uniform pressure.

For a given pressure p, the total force acting on each element is given by $p\triangle$ and its direction is always normal to the element. Then, the forces at the nodes of element i are $\mathbf{f}_i = p\triangle\mathbf{n}/3$, where $\mathbf{n}$ is the unit vector normal to element i in the current configuration, and the total load acting on a particular node of the mesh is determined by adding the contributions of all the elements connected to that node.

* Hencky (1915) obtained the value 1.713, later corrected by Campbell (1956) to 1.724.

For example, consider the total force acting at node 5, see Figure 2.2, $\mathbf{f}_5 = \mathbf{f}_{5_2} + \mathbf{f}_{5_3} + \mathbf{f}_{5_4} + \mathbf{f}_{5_6} + \mathbf{f}_{5_7} + \mathbf{f}_{5_8}$, where the second subscript corresponds to the element number.

At the the beginning of the analysis, the unstressed mesh lies in the XY plane and is unable to sustain any pressure loading, because of its zero flexural stiffness. Therefore, the equilibrium equations are singular and convergence cannot be achieved in the first step unless we first deform the membrane by imposing a small out-of-plane displacement proportional to the Hencky solution.

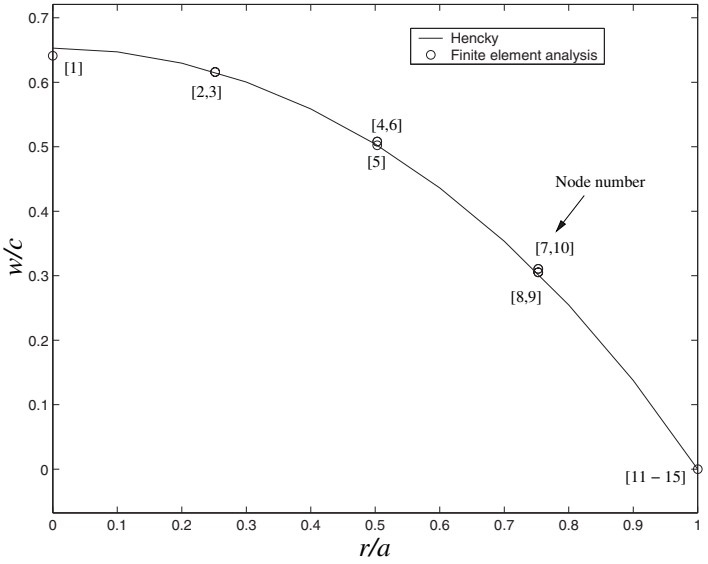

Figure 2.3: Comparison of finite element results with analytical solution.

Figure 2.3 compares the deflection of the membrane surface obtained from the Hencky solution with non-linear finite element results obtained for $a = 0.5$ m, $t = 0.02$ mm, $p = 388$ N/mm^2, E$= 2.7 \times 10^9$ N/mm^2 and $\nu = 0.3$. Note that both axes have been non-dimensionalised by plotting the non-dimensional deflexion w/c, where $c = a\,(pa/Et)^{\frac{1}{3}}$, versus the non-dimensional radius r/a. The figure shows that there is excellent agreement between the two sets of results, giving us confidence in the non-linear approach.

2.3 Cable Element

Consider the cable element $(i,\ j)$ shown in Figure 2.4. If nodes i and j have respectively displacement vectors $[U_i, V_i, W_i]^T$ and $[U_j, V_j, W_j]^T$ from the initial configuration, the strain in the cable is

$$\epsilon = \frac{l_1 - l_0}{l_0} \tag{2.15}$$

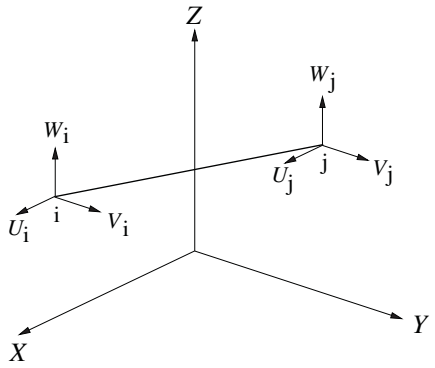

Figure 2.4: Cable element in global coordinate system.

where

$$l_0 = \sqrt{(X_j - X_i)^2 + (Y_j - Y_i)^2 + (Z_j - Z_i)^2}$$

and

$$l_1 = \sqrt{(X_j - X_i + U_j - U_i)^2 + (Y_j - Y_i + V_j - V_i)^2 + (Z_j - Z_i + W_j - W_i)^2}$$

represent the lengths of the cable element before and after deformation.

The change in strain has the following matrix expression

$$\delta\epsilon = \frac{1}{l_0}\mathbf{B}\delta\mathbf{U} \tag{2.16}$$

where the vector of *global displacement components* is

$$\mathbf{U} = [U_i \;\; V_i \;\; W_i \;\; U_j \;\; V_j \;\; W_j]^T \tag{2.17}$$

and

$$\mathbf{B} = [-C_X \;\; -C_Y \;\; -C_Z \;\; C_X \;\; C_Y \;\; C_Z] \tag{2.18}$$

contains the direction cosines of the deformed cable

$$\begin{aligned} C_X &= \frac{X_j - X_i + U_j - U_i}{l_1} \\ C_Y &= \frac{Y_j - Y_i + V_j - V_i}{l_1} \\ C_Z &= \frac{Z_j - Z_i + W_j - W_i}{l_1} \end{aligned}$$

As for the membrane element, a linear elastic constitutive relation is used

$$\sigma = E\epsilon + \sigma_0 \tag{2.19}$$

where σ_0 is the initial stress in the cable and E its Young's Modulus.

The global equilibrium equations can be obtained through the principle of virtual work. Following the same approach as in Section 2.1, but this time we use displacement and load components in the global system, we find

$$\int_{l_0} \frac{1}{l_0} \delta \mathbf{U}^T \mathbf{B}^T \sigma A dl - \delta \mathbf{U}^T \mathbf{P} = 0 \tag{2.20}$$

from which the global out-of-balance forces have the expression

$$\mathbf{\Phi}^i = \int_{l_0} \frac{1}{l_o} \mathbf{B}^T \sigma A dl - \mathbf{P} = \mathbf{B}^T \sigma A - \mathbf{P} \tag{2.21}$$

where A is the cross-sectional area.

As before, the tangent stiffness matrix consists of material and geometric contributions

$$\begin{aligned} \mathbf{K}^i &= \frac{\partial \mathbf{\Phi}^i}{\partial \mathbf{U}} \\ &= A\mathbf{B}^T \frac{\partial \sigma}{\partial \mathbf{U}} + A\sigma \frac{\partial \mathbf{B}^T}{\partial \mathbf{U}} \\ &= \frac{EA}{l_0} \mathbf{B}^T \mathbf{B} + \frac{A\sigma}{l_1} \mathbf{C} \end{aligned} \tag{2.22}$$

where

$$\mathbf{C} = \begin{bmatrix} C_Y^2 + C_Z^2 & 0 & 0 & -C_Y^2 - C_Z^2 & 0 & 0 \\ 0 & C_X^2 + C_Z^2 & 0 & 0 & -C_X^2 - C_Z^2 & 0 \\ 0 & 0 & C_X^2 + C_Y^2 & 0 & 0 & -C_X^2 - C_Y^2 \\ -C_Y^2 - C_Z^2 & 0 & 0 & C_Y^2 + C_Z^2 & 0 & 0 \\ 0 & -C_X^2 - C_Z^2 & 0 & 0 & C_X^2 + C_Z^2 & 0 \\ 0 & 0 & -C_X^2 - C_Y^2 & 0 & 0 & C_X^2 + C_Y^2 \end{bmatrix}$$

2.4 Beam Element

A full analysis of the ribs of a CRTS reflector would require a model that captures the coupling between flexural and torsional deformation, together with the associated changes in the transverse radius of curvature of the ribs. Only a detailed shell model can hope to capture such complexities; here a much simpler, equivalent rod model will be adopted.

Consider n nodal points on a curved rib, Figure 2.5, and between two consecutive nodes assume the rib to be straight, with uniform thickness t, transverse radius R, and uniform subtended angle 2α.

Unlike the membrane and cable elements, the stiffness of the rib does not change significantly within the deflection range of interest, hence it is appropriate to adopt a standard linear beam model. In this model each beam element has

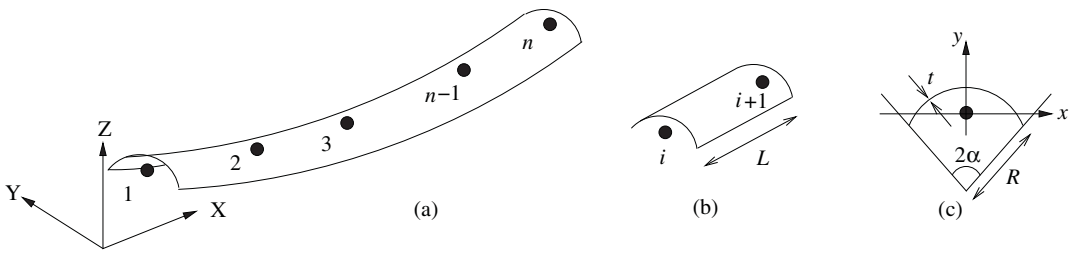

Figure 2.5: Configuration of a rib.

twelve degrees of freedom, three translation components and three rotations at each end, related to the corresponding loads by a constant stiffness matrix. Hence, the out-of-balance forces —in a local coordinate system— can be expressed as

$$\boldsymbol{\phi}^{i+1} = \boldsymbol{\phi}^{i} + \mathbf{K}\delta\mathbf{d}^{i} = 0 \tag{2.23}$$

The standard stiffness matrix of a 3D beam (Livesley 1975) is

$$\mathbf{k}_b = E \left[\begin{array}{cccccc|cccccc}
A/L & 0 & 0 & 0 & 0 & 0 & -A/L & 0 & 0 & 0 & 0 & 0 \\
0 & \frac{12I_x}{L^3} & 0 & 0 & 0 & \frac{6I_x}{L^2} & 0 & \frac{-12I_x}{L^3} & 0 & 0 & 0 & \frac{6I_x}{L^2} \\
0 & 0 & \frac{12I_y}{L^3} & 0 & \frac{-6I_y}{L^2} & 0 & 0 & 0 & \frac{-12I_y}{L^3} & 0 & \frac{-6I_y}{L^2} & 0 \\
0 & 0 & 0 & \frac{J}{2L(1+\nu)} & 0 & 0 & 0 & 0 & 0 & \frac{-J}{2L(1+\nu)} & 0 & 0 \\
0 & 0 & \frac{-6I_y}{L^2} & 0 & \frac{4I_y}{L} & 0 & 0 & 0 & \frac{6I_y}{L^2} & 0 & \frac{2I_y}{L} & 0 \\
0 & \frac{6I_x}{L^2} & 0 & 0 & 0 & \frac{4I_x}{L} & 0 & \frac{-6I_x}{L^2} & 0 & 0 & 0 & \frac{2I_x}{L} \\
\hline
-A/L & 0 & 0 & 0 & 0 & 0 & A/L & 0 & 0 & 0 & 0 & 0 \\
0 & \frac{-12I_x}{L^3} & 0 & 0 & 0 & \frac{-6I_x}{L^2} & 0 & \frac{12I_x}{L^3} & 0 & 0 & 0 & \frac{-6I_x}{L^2} \\
0 & 0 & \frac{-12I_y}{L^3} & 0 & \frac{6I_y}{L^2} & 0 & 0 & 0 & \frac{12I_y}{L^3} & 0 & \frac{6I_y}{L^2} & 0 \\
0 & 0 & 0 & \frac{-J}{2L(1+\nu)} & 0 & 0 & 0 & 0 & 0 & \frac{J}{2L(1+\nu)} & 0 & 0 \\
0 & 0 & \frac{-6I_y}{L^2} & 0 & \frac{2I_y}{L} & 0 & 0 & 0 & \frac{6I_y}{L^2} & 0 & \frac{4I_y}{L} & 0 \\
0 & \frac{6I_x}{L^2} & 0 & 0 & 0 & \frac{2I_x}{L} & 0 & \frac{-6I_x}{L^2} & 0 & 0 & 0 & \frac{4I_x}{L}
\end{array}\right] \tag{2.24}$$

where from Young (1989 p.68)

$$\begin{aligned}
I_x &= R^3 t \left[\left(1 - \frac{3t}{2R} + \frac{t^2}{R^2} - \frac{t^3}{4R^3}\right) \times \left(\alpha + \sin\alpha\cos\alpha - \frac{2\sin^2\alpha}{\alpha}\right) \right. \\
&\quad \left. + \frac{t^2 \sin^2\alpha}{3R^2\alpha(2 - t/R)} \left(1 - \frac{t}{R} + \frac{t^2}{6R^2}\right) \right] \\
I_y &= R^3 t \left(1 - \frac{3t}{2R} + \frac{t^2}{R^2} - \frac{t^3}{4R^3}\right) \times (\alpha - \sin\alpha\cos\alpha) \\
J &\approx \frac{1}{3} 2\alpha R t
\end{aligned}$$

2.5 Wrinkling

Thin membranes are unable to resist compressive stresses; instead, they form wrinkles, thus re-distributing the stresses. Following Tabarrok and Qin (1992) a simple procedure for dealing with element wrinkling has been adopted, to ensure that the simulation results are realistic.

The principal stresses σ_1 and σ_2 ($\sigma_1 > \sigma_2$) are calculated in each element, at each step of the iteration, and the following checks are then carried out

1. if $\sigma_1 \leq 0$, biaxial wrinkling occurs;
2. if $\sigma_1 > 0$ and $\sigma_2 \leq 0$, uniaxial wrinkling occurs, the wrinkles being aligned with the first principal direction;
3. if $\sigma_2 > 0$ wrinkling does not occur.

In the case of biaxial wrinkling, the element is inactive and all stresses must be set equal to zero. The elastic matrix for this element is assumed to be diagonal, with a very small stiffness s

$$\mathbf{D} = \begin{bmatrix} s & 0 & 0 \\ 0 & s & 0 \\ 0 & 0 & s \end{bmatrix} \tag{2.25}$$

For uniaxial wrinkling, the compressive stress σ_2 must be set to zero, hence

$$\boldsymbol{\sigma} = [\sigma_1 \quad 0 \quad 0] \tag{2.26}$$

and the elastic matrix *in the principal stress directions* is

$$\mathbf{D} = \begin{bmatrix} E & 0 & 0 \\ 0 & s & 0 \\ 0 & 0 & s \end{bmatrix} \tag{2.27}$$

However, note that the stress components in Equation 2.26 and the elastic matrix in Equation 2.27 need to be transformed to the element coordinate system (x, y, z) for evaluating the local element stiffness matrix. This is necessary because a wrinkled element does not behave isotropically.

Chapter 3

CRTS Reflector Assembly

3.1 Overall Procedure

The analysis presented in this chapter is divided into three stages: i. rotation of (flat) membrane gores; ii. connection of gores and edge cables to the ribs; 3) determination of the actual surface.

Figure 3.1 shows the first two stages, schematically. A single gore ABCD, whose edges are shaped according to the cutting pattern computed by Lai, You and Pellegrino (1997), initially lies in the XY plane with a cable attached to the top edge. This cable is held stretched by end forces T, since the top edge of the membrane is longer than the unstressed cable.

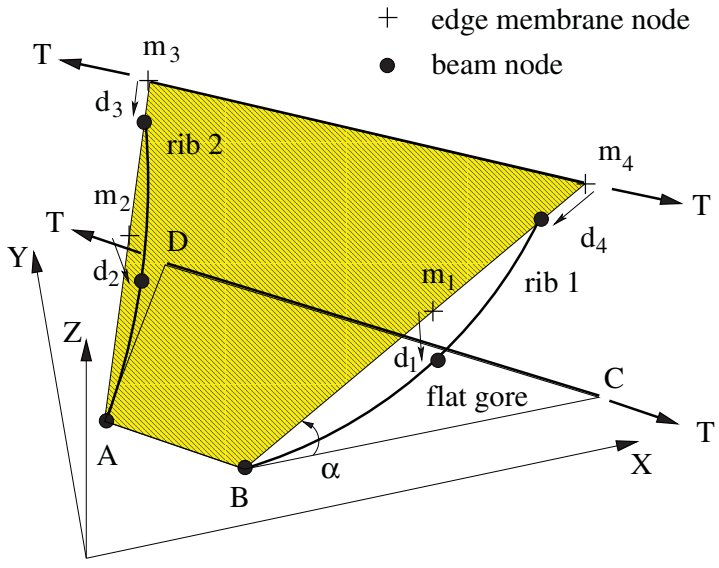

Figure 3.1: Connecting the membrane to the ribs (assumed to be rigid).

First, the gore and cable are rotated as a rigid body about AB, through an angle α such that a straight line through B and C passes through the tip and

root of a rib.

Second, each of the nodes along the edges of the membrane, in the figure m_1, m_2, m_3, m_4, is assigned a displacement such that each node moves to the corresponding position on the rib. The shape of the membrane surface with its edges attached to the ribs —assumed to be rigid at this stage— is computed by carrying out a series of equilibrium iterations. This is repeated for each gore and the shape obtained at the end is doubly-curved in each gore, but is not the actual shape of the reflector because the ribs have not been allowed to deform elastically.

Finally, when all ribs have been separately analysed, the actual shape of the reflector is determined by removing the constraints on the ribs and performing a series of global equilibrium iterations.

The main reason for dividing the analysis into these three separate steps is that, by achieving convergence to two intermediate configurations, the chances of converging in the final iteration are much increased.

3.2 Phase I - Rotation of Membrane

Figure 3.2 shows the sequence of rotations of a gore. First, the cutting pattern for the gore is generated in the local coordinate system xy and it is rotated through an angle α about the x-axis, then it is rotated through an angle β about Z, such that corners A and B of the gore are in their required positions on the reflector surface.

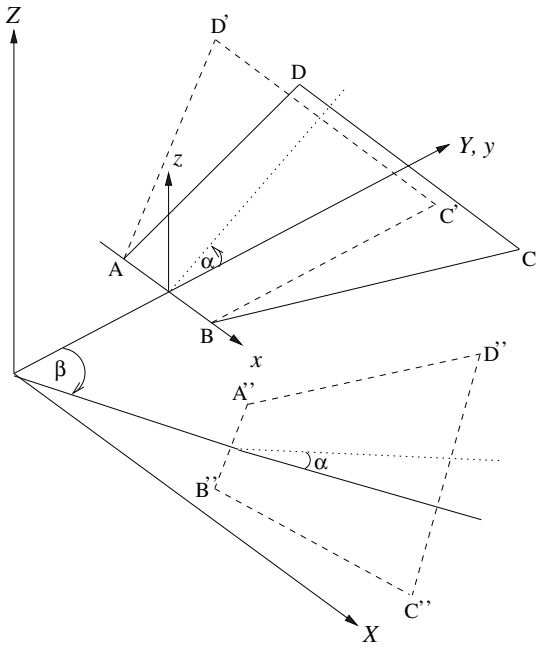

Figure 3.2: Rotation of a gore.

The calculation of α has been discussed in Section 3.1, and $\beta = 2(i-1)\pi/g$, where g is the total number of gores in the reflector and i is the particular gore that is being analysed. The transformation of the nodal coordinates is

$$\begin{bmatrix} X \\ Y \\ Z \end{bmatrix} = \begin{bmatrix} \cos\beta & \sin\beta & 0 \\ -\sin\beta & \cos\beta & 0 \\ 0 & 0 & 1 \end{bmatrix} \begin{bmatrix} 1 & 0 & 0 \\ 0 & \cos\alpha & -\sin\alpha \\ 0 & \sin\alpha & \cos\alpha \end{bmatrix} \begin{bmatrix} x \\ y \\ 0 \end{bmatrix} \tag{3.1}$$

3.3 Phase II - Membrane Attached to Ribs

At the end of Phase I the edge nodes of each gore are attached to the hub. Then, one gore at a time, each node on a side edge of the gore is assigned a displacement vector such that the node moves to the corresponding position on the rib.

This is done by modifying the stiffness equations of the nodes whose displacements have been prescribed. Because these displacements are no longer unknown, they are multiplied by the corresponding columns of the global stiffness matrix and then moved to the right-hand-side of the stiffness equations. The corresponding equations are eliminated. It has been found that in some cases these displacements have to be imposed in several steps, to avoid convergence problems.

When this is done, all the nodes are in equilibrium except for those that are attached to the ribs, which were not included in the equilibrium equations.

3.4 Phase III - Computation of Actual Surface

In Phase II all the cable and beam nodes were fully connected to the corresponding membrane nodes, but in the real reflector each rib is accommodated within a membrane pocket and the cable is covered by a Nylon sheath that allows sliding. Phase II allows this sliding to take place, and also removes all residual constraints on the reflector.

Figure 3.3 illustrates the modelling of these sliding contacts. For clarity, the three types of elements —membrane, cable and beam— are shown separately. Sliding between a beam/cable node and its corresponding membrane node occurs in the direction of the local tangent to the beam/cable, see for example the enlarged picture of the sliding direction $s2$ in Figure 3.3. Sliding constraints are applied by modifying the equilibrium equations of the nodes involved, as follows.

For example, consider cable element $c1$. Its equilibrium equation has the form

$$[\mathbf{K}^8_{c1} \mid \mathbf{K}^9_{c1}] \begin{bmatrix} \mathbf{d}_{8c} \\ \mathbf{d}_{9c} \end{bmatrix} = \begin{bmatrix} \mathbf{P}_{8c_1} \\ \mathbf{P}_{9c_1} \end{bmatrix}, \tag{3.2}$$

Because at node 8 the cable and membrane nodes coincide,

$$\mathbf{d}_{8c} = \mathbf{d}_{8m} \tag{3.3}$$

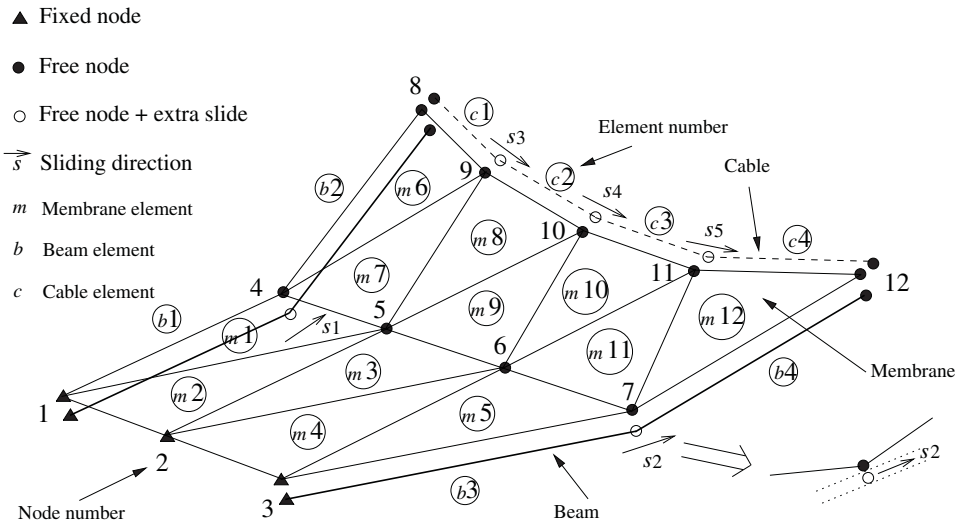

Figure 3.3: Schematic view of gore with sliding elements.

On the other hand, the displacement of cable node 9 is related to the corresponding membrane node by

$$\mathbf{d}_{9c} = \mathbf{d}_{9m} + \delta_3 \mathbf{s}_3 \tag{3.4}$$

where δ_3 is the unknown magnitude of the sliding between the cable node and the membrane node, and $\mathbf{s}_3$ is the sliding direction

$$[\mathbf{K}^8_{c1} \mid \mathbf{K}^9_{c1} \mid \mathbf{K}^9_{c1}\mathbf{s}_3] \begin{bmatrix} \mathbf{d}_{8m} \\ \mathbf{d}_{9m} \\ \delta_3 \end{bmatrix} = \begin{bmatrix} \mathbf{P}_{8c_1} \\ \mathbf{P}_{9c_1} \end{bmatrix} \tag{3.5}$$

Equations similar to Equation 3.5 can be obtained for all other sliding nodes, thus formulating all stiffness equations in terms of only membrane nodal displacements. For the example shown in Figure 3.3 five extra variables $\delta_1, \ldots \delta_5$ are introduced by doing this. Obviously, the resulting stiffness matrix is no longer square and hence five additional equations are needed.

These additional equations are obtained by noting that the three-dimensional external load vector for node i, shown in Figure 3.4 and containing an internal, frictionless slider, consists of four components. These components can be taken as either $\mathbf{P}_{ic}$ and R or $\mathbf{P}_{im}$ and R, depending on whether the equations are being formulated in terms of cable or membrane degrees of freedom. Note that the nodal loads can be converted to membrane components with

$$\mathbf{P}_{im} = \mathbf{P}_{ic} + R\mathbf{s} \tag{3.6}$$

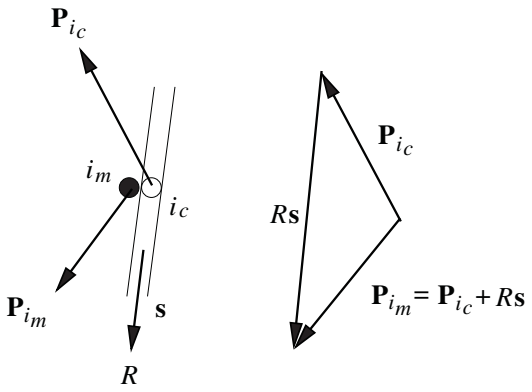

Figure 3.4: External loads on node with internal slider.

In all five sliding nodes of the CRTS reflector it has been assumed that $R = 0$. Hence, for the example shown in Figure 3.3 the five additional equations have been obtained by taking the dot-product of Equation 3.6 with $\mathbf{s}_i$ for these nodes.

Considering the elements actually connected to these five nodes one obtains

$$\begin{aligned}
(\mathbf{P}_{4b_1} + \mathbf{P}_{4b_2} - \mathbf{P}_{4m_1} - \mathbf{P}_{4m_6} - \mathbf{P}_{4m_7}) \cdot \mathbf{s}_1 &= 0 \\
(\mathbf{P}_{7b_3} + \mathbf{P}_{4b_4} - \mathbf{P}_{4m_5} - \mathbf{P}_{4m_{11}} - \mathbf{P}_{4m_{12}}) \cdot \mathbf{s}_2 &= 0 \\
(\mathbf{P}_{9c_1} + \mathbf{P}_{9c_2} - \mathbf{P}_{9m_6} - \mathbf{P}_{9m_7} - \mathbf{P}_{9m_8}) \cdot \mathbf{s}_3 &= 0 \\
(\mathbf{P}_{10c_2} + \mathbf{P}_{10c_3} - \mathbf{P}_{10m_8} - \mathbf{P}_{10m_9} - \mathbf{P}_{10m_{10}}) \cdot \mathbf{s}_4 &= 0 \\
(\mathbf{P}_{11c_3} + \mathbf{P}_{11c_4} - \mathbf{P}_{11m_{10}} - \mathbf{P}_{11m_{11}} - \mathbf{P}_{11m_{12}}) \cdot \mathbf{s}_5 &= 0
\end{aligned} \tag{3.7}$$

Each of the terms inside the brackets can be expressed as the product of a stiffness matrix multiplied by some displacement component, e.g. Equation 3.5, and hence Equation 3.7 can be written in terms of the same membrane displacement variables and sliding displacements considered above. For the example shown in Figure 3.3 this yields the following system of stiffness equations

$$\mathbf{K}_{(44\times 44)} \begin{bmatrix} \mathbf{d}_{4m} \\ \mathbf{d}_{5m} \\ \vdots \\ \mathbf{d}_{12m} \\ \delta_1 \\ \vdots \\ \delta_5 \\ \theta_4 \\ \vdots \\ \theta_{12} \end{bmatrix}_{(44\times 1)} = \begin{bmatrix} \mathbf{P}_{4m} \\ \vdots \\ \mathbf{P}_{12m} \\ 0 \\ \vdots \\ 0 \\ M_4 \\ \vdots \\ M_{12} \end{bmatrix}_{(44\times 1)} \tag{3.8}$$

Note that this system of equations has 44 degrees of freedom, consisting of $9 \times 3 = 27$ displacement components, plus $4 \times 3 = 12$ rotation components and 5 for the sliding displacements.

For offset reflector configurations, half of the reflector needs to be considered in the above analysis, because there is only one symmetry plane (Lai and Pellegrino 1999). However, it should be noted that, if the two ribs in the symmetry plane are given identical properties to the others, the out-of-balance loads applied to the nodes on these ribs, which correspond to only half of the reflector, need to be doubled.

3.5 Simulation Algorithm

The simulation procedure outlined above has been implemented in a series of Matlab m-files. In Phase II and Phase III the convergence criterion is that the norm of the out-of-balance forces should be smaller than 10^{-4} [N].

The overall layout of the simulation is presented in Figure 3.5.

Figure 3.5: Flow chart of simulation algorithm.

Chapter 4

Results

4.1 Introduction

Severe convergence problems were encountered in running the simulation described in the previous chapter. In particular, the out-of-balance loads associated with the sliding elements described in Section 3.4 showed such poor convergence converge that the sliding boundaries had to be removed.

This chapter compares the results of non-linear finite-element simulations of two offset reflectors, whose configurations parameters are given in Table 4.1, with the results of a linear analysis of the same reflectors.

No. of ribs	8, 12
Diameter	1 m
F/D	0.9
Offset A	0.1 m
Prestress t_x	40 N/m
Prestress t_y	10 N/m

Table 4.1: Details of reflectors analysed.

As the non-linear finite-element simulation provides some insight into the behaviour of CRTS reflectors. Therefore, intermediate results at the end of Phase II are presented, as well as the end of the analysis. Also, since the 12-rib reflector did not converge at the end of Phase III, the intermediate results are all that is available.

4.2 Phase II Results

It normally required less than ten Newton-Raphson iterations for the analysis to converge. The key results including both the principal stresses and surface error distribution for both reflectors, are shown in Figure 4.1. Table 4.2 gives the

corresponding RMS error, with respect to a best fit paraboloid of equation

$$Z = a(X^2 + Y^2) + b \tag{4.1}$$

and the corresponding values obtained from the "Linear Analysis", i.e. the method described in Lai and Pellegrino (1999).

After the Phase II iteration, the surface is fairly close to the equilibrium surface, since the displacement of the ribs is quite small.

Configuration		RMS error [m]	a [m^{-1}]	b [m]
8 ribs	Linear Analysis	0.0026	0.2785	0.0024
	NLFE	0.0021	0.2778	0.0012
12 ribs	Linear Analysis	0.0013	0.2782	0.0007
	NLFE	0.0010	0.2780	0.0002

Table 4.2: RMS errors and best-fit paraboloid parameters after Phase II.

4.3 Phase III Results

Figure 4.2 shows plots of the norm of the out-of-balance forces, $||\phi||$, during the Newton-Raphson iteration. For the 8-rib reflector $||\phi||$ decreases to less than 50 N in about 100 iterations, and then to a very small value after several more iterations. The corresponding plot for the 12-rib reflector showed huge fluctuations and hence, instead of plotting $||\phi||$, Fig. 4.2 (b) shows a plot of $\ln ||\phi||$. In this case convergence was not achieved, and hence the actual shape of the reflector could not be found.

Therefore, only for the 8-rib reflector we are able to compare the non-linear finite-element analysis with the linear analysis. Figure 4.3 shows the principal stress and surface error distribution from the two analyses. Note that the stresses along the edge of the surface are almost double according to the non-linear finite element simulation, but this may well be due to the fixed boundary conditions assumed between the membrane and the cables/beams. The direction of the principal stresses has hardly changed. Regarding the distribution of the surface errors, there is very little difference between the linear and non-linear predictions.

Table 4.3 compares the RMS errors of the surfaces obtained from the linear and non-linear methods. The coefficients of the best-fit paraboloid are a little different, but the RMS errors are practically identical.

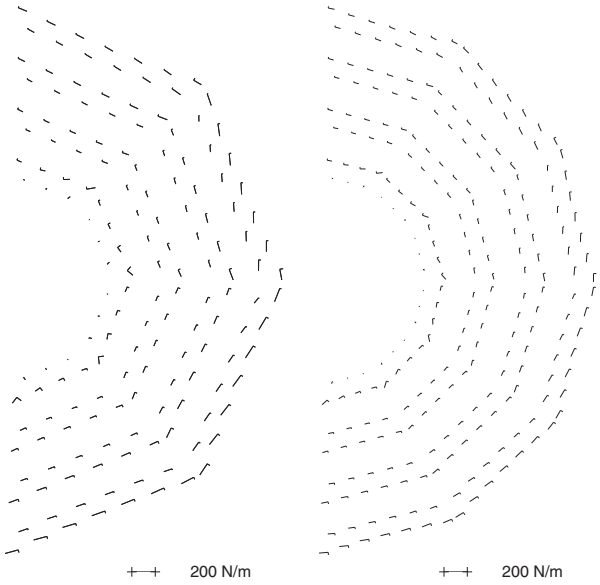

(a) 8 ribs (b) 12 ribs

Principal stresses

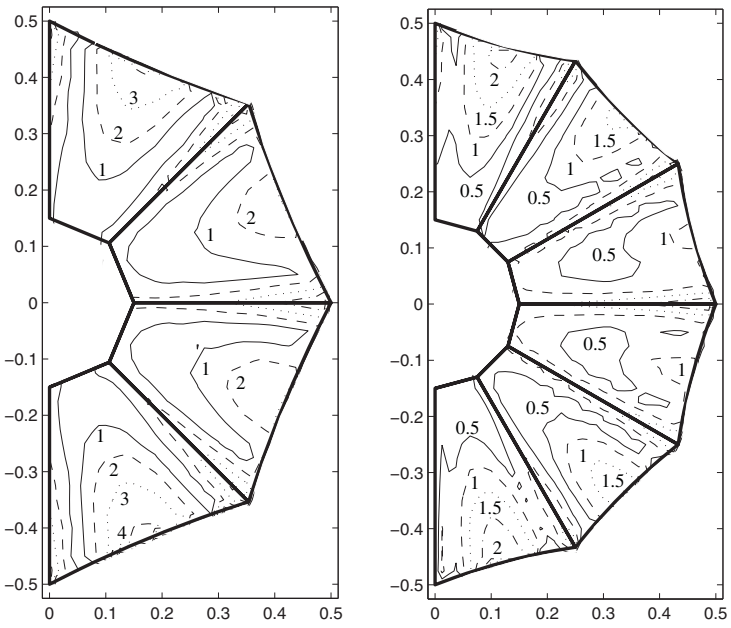

(c) 8 ribs (d) 12 ribs

Error (mm)

Figure 4.1: Principal stress and surface error distribution after Phase II.

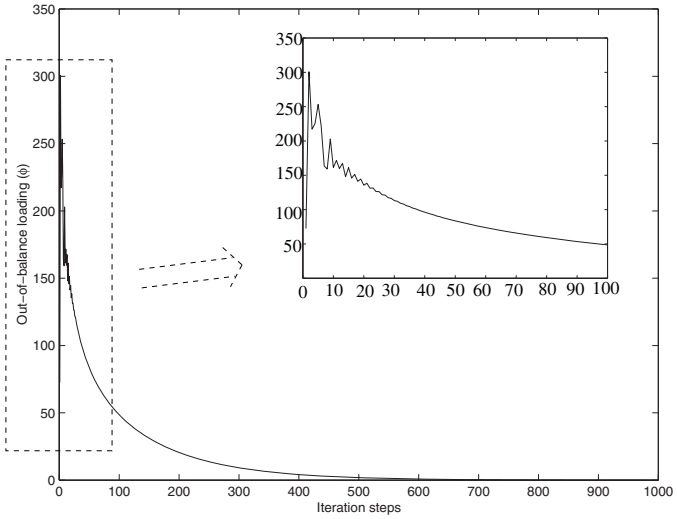

(a) 8 ribs

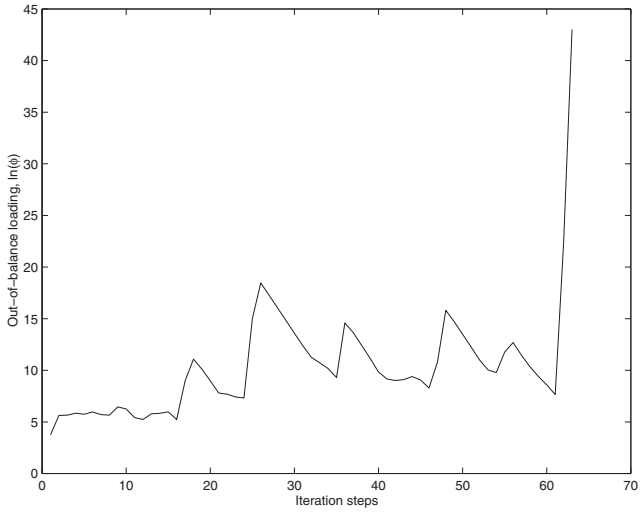

(b) 12 ribs

Figure 4.2: Norms of out-of-balance loads, $||\phi||$, during Newton-Raphson iteration.

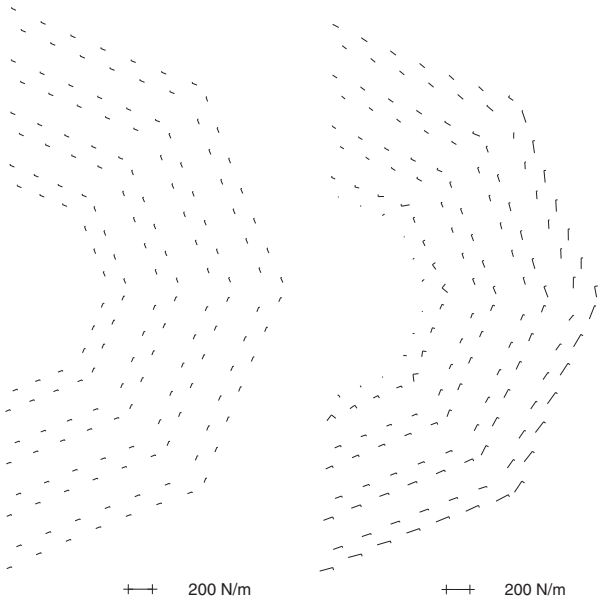

(a) Linear Analysis (b) NLFE

Principal stresses

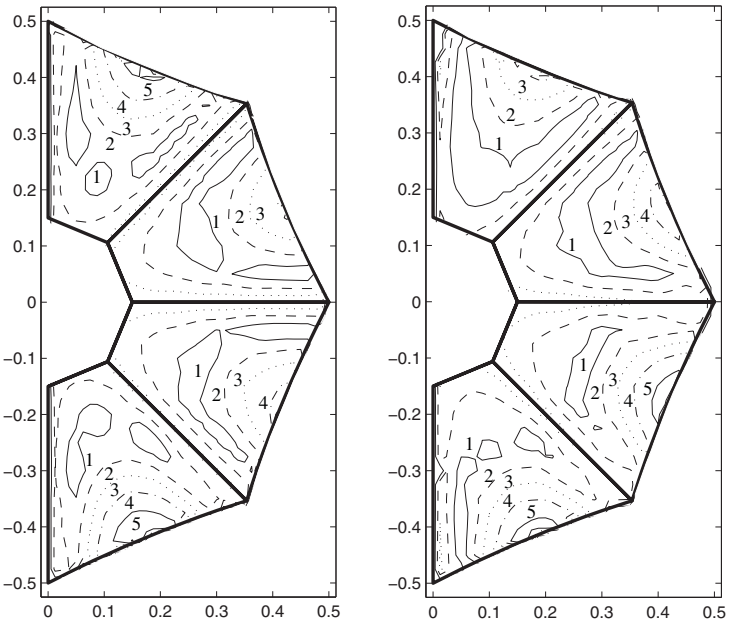

(c) Linear Analysis (d) NLFE

Surface error

Figure 4.3: Principal stresses and surface error distribution from linear and non-linear analyses.

	RMS error [m]	a [m^{-1}]	b [m]
Equilibrium surface	0.0026	0.2785	0.0024
Actual surface (Linear Analysis)	0.0026	0.2785	0.0024
Actual surface (NLFE)	0.0025	0.2762	0.004

Table 4.3: Comparison of RMS errors for 8-rib reflector.

Chapter 5

Discussion

The development of a proper simulation of the assembly process and prestressing of an offset CRTS reflector has turned out to be a formidable computational challenge. Special purpose simulation software had to be developed and, despite this, it was possible to obtain only a limited set of results.

A complete non-linear simulation of an 8-rib offset reflector with $F = 0.9$ m and $D = 1$ m was carried out and the results have been compared to a linear analysis carried out with the software described in Lai and Pellegrino (1999). The RMS surface error predicted by the two methods is practically identical but, although the principal stress directions match pretty well, discrepancies of up to 100% in the stress magnitudes have been observed. The likely reason for this is that in the non-linear simulation sliding between the membrane and the cables and ribs could not be properly modelled. This is a topic that remains open for further investigation.

It is concluded that the linear-elastic analysis method of Lai and Pellegrino (1999) is a very good way of determining the actual prestressed shape of a CRTS reflector.

Bibliography

Belytschko, T., Liu, W. K. and Moran, B. (2000). *Nonlinear Finite Elements for Continua and Structures*. J. Wiley & Sons, Chichester.

Campbell, J. D. (1956). On the the theory of initially tensioned circular membranes subjected to uniform pressure. *Quarterly Journal of Mech. and Applied Math.*, Vol. IX, Pt. 1, pp. 84-93.

Crisfield, M. A. (1991). *Non-linear finite element analysis of solids and structures. Volume 1: essentials*. John Wiley & Sons, Chichester.

Hencky, H. (1915). Uber den Spannungsztand in Kreisrunden Platten mit verschwindender Biegungssteifigkeit. *Z. fur Math. and Physik*, Vol. 63, pp. 311-317.

Lai, C. Y., You, Z., Pellegrino, S. (1997). *Shape and stress analysis of symmetric CRTS reflectors*. CUED/D-STRUCT/TR170. University of Cambridge.

Lai, C. Y., Pellegrino, S. (1999). *Shape and Stress Analysis of Offset CRTS reflectors*. CUED/D-STRUCT/TR177. University of Cambridge.

Livesley, R. K. (1975). *Matrix Methods of Structural Analysis*, Second Edition, Pergamon Press, Oxford.

Love, A. E. H. (1944). *A treatise on the mathematical theory of elasticity.*, Fourth Edition, Dover Publications, New York.

Tabarrok, B. and Qin, Z. (1992). Nonlinear analysis of tension structures, *Computers & Structures*, Vol. 45, No. 5/6, pp. 973-984.

Young, W. C. (1989). *Roark's Formulas for stress and strain*, Sixth Edition, McGraw-Hill, New York.